Capillary transport in paper porous materials at low saturation levels: normal, fast or superfast?

Article

Accepted Version

Capillary transport in paper porous materials at low saturation levels: normal, fast or superfast?

Alex V. Lukyanov*
School of Mathematical and Physical Sciences, University of Reading, Reading, RG6 6AX, UK

Vladimir V. Mitkin
Aerospace Research Laboratory, University of Virginia, Charlottesville, VA 22903, USA

Tristan Pryer
Department of Mathematical Sciences, University of Bath, Bath, BA2 7AY, UK

Penpark Sirimark
Department of Science and Mathematics, Rajamangala University of Technology Isan, Surin, Thailand

Theo G. Theofanous
University of California, Santa Barbara, CA 93106, USA

The problem of capillary transport in fibrous porous materials at low levels of liquid saturation has been addressed. It has been demonstrated, that the process of liquid spreading in this type of porous materials at low saturation can be described macroscopically by a similar super-fast, non-linear diffusion model as that, which had been previously identified in experiments and simulations in particulate porous media. The macroscopic diffusion model has been underpinned by simulations using a microscopic network model. The theoretical results have been qualitatively compared with available experimental observations within the witness card technique using persistent liquids. The long-term evolution of the wetting spots was found to be truly universal and fully in line with the mathematical model developed. The result has important repercussions on the witness card technique used in field measurements of dissemination of various low volatile agents in imposing severe restrictions on collecting and measurement times.

I. INTRODUCTION

Liquid distributions and transport in particulate porous media, such as clay, loam and sand, at low saturation levels was found to have very distinctive features resulting in a special class of mathematical problems, superfast non-linear diffusion [1–4]. It has been established, both experimentally and theoretically, that any time, any wetting liquid naturally (that is when there is no force wetting regime involved) spreads in a dry (or a nearly dry) porous particulate matrix, the moving front dynamics follows, after some time, the power evolution law dictated by the superfast non-linear diffusion mechanisms [1, 4].

The special character of this non-linear diffusion process is caused by the loss of global, pore-scale connectivity at low levels of saturation. In this case, the liquid transport only occurs over the surface elements of the porous matrix, sand particles for example, while the liquid is mostly located in the capillary bridges formed at the point of particle contacts.

In terms of the mathematical structure, the superfast nonlinear diffusion equation has the coefficient of diffusion, which demonstrates nearly divergent behaviour as a function of the porous matrix saturation s, $D(s) \propto (s - s_0)^{-3/2}$, leading to hyperdispersive character of the spreading process [5]. This is in contrast to the mathematical formulations involving the standard porous medium equation, where the coefficient of diffusion $D(s)$ is either a constant (leading to normal, Gaussian dispersive behaviour) or a monotonically decreasing function ($D(s) \propto s^m, m > 0$, leading to hypodispersive behaviour) [6]. The empirical models widely used in practice to simulate flow in various soils have much more complicated algebraic structure, but do not describe low saturation regime where the divergent behaviour is expected [7, 8].

Note, s_0 is some minimal saturation level ($s_0 \approx 1\%$), which could be only achieved, hypothetically, in a state when the liquid bridges completely cease to exist [1, 4, 9, 10]. Obviously, the liquid bridges always exist in the simulation domain to enable the transport. Therefore, condition $s > s_0$ should be satisfied, and the singularity, strictly speaking, does not exist, though s can come very close to the minimal value s_0 [1, 4].

For the first time, the diverging behaviour of the diffusion coefficient $D(s)$, named *hyperdispersion*, was predicted in the analysis of spreading in porous networks driven by the disjoining pressure [11]. Later on, unusual mathematical properties of the fast ($-1 \leq m < 0$) and superfast ($m < -1$) diffusion equations were noticed in the analysis of various physical processes ranging from

* corresponding author,
a.lukyanov@reading.ac.uk

transport in hot magnetized plasmas to non-Markovian effects taking place in some porous matrices [12, 13].

Apparently, liquid spreading in dry porous materials is not just characteristic for particulate porous media, such as sand, but also frequently occurs in other porous materials. Therefore, in this paper, the previously developed model [1–4] is generalized to another fairly common type of porous materials consisting of fibre elements, such as papers and textiles, where a similar kind of non-linear diffusion process is anticipated. We would like to understand how general and universal the superfast mechanism, first discovered in particulate porous media [1], actually is. We note that this transport regime is important for many medical applications, since it commonly occurs in chromatographic flows and lateral flow test setups widely used in the infectious disease testing [14–16].

II. MACROSCOPIC AND MICROSCOPIC MODELS OF CAPILLARY TRANSPORT IN FIBER POROUS MATERIALS

The structure of fibrous porous materials is quite different from that of particulate porous media [17–22]. Yet, all the main elements of the superfast diffusion (SFD) model can be identified here too.

At low saturation levels, the liquid is only located on the surfaces of the fibres (including intrafibre pores) and in the liquid bridges formed at the intersections of the fibres [23–25]. The microscopic surface details, such as roughness, generate the capillary pressure to drive the liquid flow through the network, where the liquid bridges, as in the case of particulate media, play the role of variable volume reservoirs. We further assume that the liquid at least partially wets the fibres, so that the contact angle on the rough surfaces of the fibres would be small (close to zero) or zero.

As in the previous case of particulate porous media [4], we first consider the morphology of the liquid distribution in fibrous materials at low saturation levels to formulate a pressure-saturation relationship, which will be further used to obtain a macroscopic, average model. The macroscopic model parameters will be assessed and analysed with the help of a microscopic network setup, which, in parallel, will serve to underpin and strengthen the macroscopic formulation and its hypothesis. In the end, we consider a set of available experimental data, and compare the general trends expected from the macroscopic formulation with the experimental results. We will demonstrate and discuss the weaknesses and shortcomings of the previous measurements.

A. Quasi-steady liquid distribution in fibrous materials at low saturation levels

The morphology of the liquid structures formed between the crossing fibres (or nearly crossing fibres with the shortest distance between them being smaller than the fibre diameter) in the wetting case is found to be in general more complex than that observed between the particles [9, 10, 22–25].

In particulate porous media, isolated bridges only exist below a certain critical level of saturation $s \leq s_c \approx 8-10\%$, where the saturation s is defined as the ratio of the liquid volume V_L to the available volume of voids V_E, $s = \dfrac{V_L}{V_E}$ in a sample volume V. Above the critical level, isolated bridges coalescence into larger clusters, such as trimmers, pentamers and more complex agglomerates. This trend has been observed for idealized systems consisting of spherical grains and for non-spherical particle media, like real sand [9].

In fibrous porous media, the liquid volume at the crossing of two rigid fibres can take under the action of surface tension forces several distinct morphologies depending on the amount of the liquid V_B, the separation distance and the angle between the fibres θ_f. Namely, one may observe a long liquid column, a mixed morphology state that consists of a drop on one side together with a small amount of liquid on the other side and a drop or a compact hemispherical drop or a pendular ring [23–25]. In general, the elongated liquid columns are only formed at small angles $\theta_f \leq 20^\circ$ between the crossing fibres [24]. So that the predominant shape of the liquid volumes in randomly oriented fibrous materials appears to be either a drop or a pendular ring at small saturation levels $s \leq s_c$.

The shape of an isolated bridge (a pendular ring) can be determined analytically in a closed form only in quasi-static conditions and in a simplified geometry, for example in the case of two spheres in contact or at small separating distances [26]. The analytic forms are lengthy, but approximately results in the following scaling of the capillary pressure in the liquid bridge p as a function of its volume V_B

$$p \approx -p_0 \left(\frac{R^3}{V_B}\right)^{\gamma_p}, \quad \gamma_p \approx 1/2. \tag{1}$$

Here, the length scaling parameter R could be either the diameter of the spherical particle (in particulate porous media) or the characteristic fibre thickness, $p_0 = \frac{4\gamma}{R}$ and γ is the coefficient of surface tension of the liquid [1, 4, 9, 27]. The scaling law can be applied at low levels of saturation $s \leq s_c$, even for particulate media consisting of non-spherical particles, such as sand, before the capillary pressure saturates at a universal critical value [9]. As a result, in what follows, relationship (1) is taken as the main pressure scaling law in capillary bridges at fibre crossings in our model. The scaling law (1) is expected to be violated only if the dominant morphology of the liquid volumes would change from a drop (or a pendular ring) to elongated columns.

B. Macroscopic and microscopic parameters of fibrous materials

We note that the connectivity of fibres in a porous material (the main morphology of the crossings) can be also in a form of a branch, when each crossing has three links coming out instead of four as in the case of a common crossing, Fig. 1.

The porosity of fibrous materials ϕ is highly variable (one can easily change paper porosity by applying moderate mechanical pressure to a sample), and, in general, it is much higher than that of particulate porous media. The typical porosity values for most paper grades are found to be around $\phi = 0.7$ (sand porosity, in comparison, is around $\phi = 0.3$) [21]. The larger porosity values imply that overlapping (coalescence) of the liquid volumes attached to different crossings (the effect observed in particulate porous media [9, 22]) may only occur at much larger values of saturation.

It is well known that the structure of fibrous materials is effectively two-dimensional, that is the fibres are roughly oriented in the paper sheet plane. The main characteristics of the paper materials are therefore also two-dimensional, such as the total length of fibres L_q per unit area of a paper sheet. Typically, it takes the values in between $200 \le L_q \le 400\,\mathrm{mm}^{-1}$ at the characteristic paper thickness around $50\,\mu$m [20]. Given the characteristic fibre thickness R in the range $4\,\mu\mathrm{m} \le R \le 10\,\mu\mathrm{m}$, one can define the total length of fibres L_e per unit area in a layer of thickness R, which is expected in the range of $16 \le L_e \le 80\,\mathrm{mm}^{-1}$. The so-obtained typical range is consistent with the typical paper porosity levels. Indeed, $\phi = \frac{V_E}{V}$, that is $\phi = 1 - \pi L_e R/4$ in a sample volume V of thickness R assuming circular fibre cross-section area $\pi R^2/4$. The estimate then gives $\phi \approx 0.7$, if we take parameters in the middle of their expected, estimated intervals, that is $L_e = 50\,\mathrm{mm}^{-1}$ and $R = 7\,\mu$m. This implies that parameters ϕ, L_e and R characterising porous network are always interrelated.

C. Macroscopic model

To characterise liquid distributions macroscopically, one needs to introduce quantities averaged over a sufficiently large volume element. In what follows, we will briefly follow the procedure similar to that in [4], while binding parameters to the specific case of fibrous materials and defining their characteristic values.

First, an average coordination number, that is the average number of crossings per unit volume N_c is to be defined. The value of L_e in a random paper network allows to estimate the mean distance l_f between the nearest fibre crossings, as in [20], $l_f \approx \frac{2}{\pi L_e}$. That is, typical values of l_f are expected in the range $8\,\mu\mathrm{m} \le l_f \le 13\,\mu$m. Using $R = 7\,\mu$m and $L_e = 50\,\mathrm{mm}^{-1}$, one can obtain an estimate of the coordination number with a typical value $N_c = \frac{\pi L_e^2}{2R} \approx 5.6 \times 10^5\,\mathrm{mm}^{-3}$.

To parametrize saturation, we split, similar to [4], average liquid content in a sample volume $V = S_0 R$ of thickness R and surface area S_0 into two parts: the liquid contained on the rough surface of fibres and in the intrafibre pores of volume $V_r = L_e S_0 \delta_R^2$ and the liquid contained in the capillary bridges at the fibre crossings $V_c = V_B N_c V$.

The parameter δ_R has the dimension of length and could be considered as the fitting parameter of the model. It can be interpreted as the characteristic length scale of the surface roughness (intrafibre pore size). We further assume that the smaller details (on the length scale $L \ll R$) of fibres are fully saturated, as it is commonly found on the rough surfaces [28], such that the amount of the liquid stored on the rough surface of fibres and in the intrafibre pores is independent of the liquid pressure, that is constant. This approximation is well fulfilled if the capillary pressure is on the scale of $p \approx p_0$.

Combining both contributions, saturation

$$s = \frac{V_c + V_r}{\phi V}$$

can be presented as

$$s = V_B V_0^{-1} + s_0, \quad V_0 = \frac{\phi}{N_c}, \tag{2}$$

where

$$s_0 = \frac{L_e \delta_R^2}{\phi\, R}$$

is the saturation level when all liquid bridges cease to exist. Note, within the wet area one has always that $V_B > 0$, so that $s > s_0$.

Then, using (2), the average capillary bridge pressure $P =< p >^l$

$$P = -p_0 \left(\frac{R^3}{V_0}\right)^{1/2} \frac{1}{(s - s_0)^{1/2}}, \tag{3}$$

where $< ... >^l = V_l^{-1} \int_{V_l} dx_1 dx_2 dx_3$ is intrinsic liquid averaging, V_l is liquid volume within the sample volume V. Using $L_e = 50\,\mathrm{mm}^{-1}$, $\delta_R = 1\,\mu$m, $R = 7\,\mu$m and $\phi = 0.7$ as the typical parameters, one can estimate that the residual saturation level $s_0 \approx 10^{-2}$, that is about 1% as expected.

Consider now local transport on the surface of fibres and in the intrafibre pores. The surface flux density $\mathbf{q}$, according to the previous study of liquid spreading on rough surfaces made of microscopic grooves of various shapes and dimensions [28], obeys a Darcy-like law

$$\mathbf{q} = -\frac{\kappa_m}{\mu} \nabla \psi, \tag{4}$$

where μ is liquid viscosity, ψ is local pressure in the liquid averaged within the surface roughness and $\kappa_m = \kappa_0 \delta_R^2$

is the effective coefficient of permeability of the surface roughness, which is proportional to the square of the length scale parameter δ_R. In the assumption of fully saturated fibres, $\kappa_m = const$.

According to the spatial averaging theorem [29], applying intrinsic liquid averaging $< ... >^l$

$$-\frac{\kappa_m}{\mu}\left\{\nabla < \psi >^l + V_l^{-1}\int_{S_l}\psi\,\mathbf{n}\,dS\right\} =< \mathbf{q} >^l, \quad (5)$$

where S_l is the area of liquid interface with normal vector $\mathbf{n}$. The surface integral in the creeping flow conditions, when the pressure variations across the liquid layer are insignificant, can be neglected $V_l^{-1}\int_{S_l}\psi\,\mathbf{n}\,dS \approx 0$ and

$$-\frac{\kappa_m}{\mu}\nabla < \psi >^l =< \mathbf{q} >^l . \quad (6)$$

Now, one can cast the continuity equation, in the absence of evaporation,

$$\frac{\partial(\phi s)}{\partial t} + \nabla\cdot\mathbf{Q} = 0$$

into

$$\frac{\partial(\phi s)}{\partial t} = \nabla\cdot\left\{\frac{K}{\mu}\nabla P\right\}. \quad (7)$$

Here,

$$\mathbf{Q} = \frac{S_e}{S} < \mathbf{q} >^l, \quad (8)$$

S is the surface area of the sample volume V with the effective area of entrances and exits S_e and coefficient $K = \kappa_m\frac{S_e}{S}$. Also, it has been assumed that in the creeping flow conditions $P =< p >^l \approx < \psi >^l$. Note, that the ratio S_e/S is not strictly speaking just a geometric factor. It is an average quantity defined by (8), which incorporates connectivity and the shape of the surface elements.

Assuming further that porosity ϕ is constant and using expression (3) for the average pressure, one can transform the governing equation (7) into a non-linear diffusion equation for the saturation $s(\mathbf{x}, t)$

$$\frac{\partial s}{\partial t} = \nabla\cdot\left\{\frac{D_0\,\nabla s}{(s-s_0)^{3/2}}\right\}, \quad (9)$$

where

$$D_0 = \frac{1}{2}\frac{K}{\mu}\frac{p_0}{\phi}\left(\frac{R^3}{V_0}\right)^{1/2}.$$

The resultant non-linear diffusion equation (9) has a similar form as that studied in [1, 4] in the case of particulate porous media. The main difference at this point is that the equation in the bulk has a constant coefficient of diffusion D_0, which is defined by the connectivity of the porous network of fibres, while in particulate porous media, there is a weak logarithmic dependence on saturation, and the diffusivity is driven by the shape of the particles and their contact area, details can be found [1–4]. In a way, the situation is simpler in the case of fibrous materials than that in particulate media, since the connectivity parameter can be quite accurately found via a network model. This will be done in the next part of this study. On the other hand, the question of the liquid amount stored in the intrafibre space is still open, and down to simplifying assumptions at this stage.

To address a moving boundary value problem set in an open domain with a smooth boundary $\partial\Omega$ moving with velocity $\mathbf{v}$, the governing equation (9) can be complemented with the boundary conditions

$$s|_{\partial\Omega} = s_f, \quad s_f > s_0 \quad (10)$$

and

$$\mathbf{v}\cdot\mathbf{n} = -D_0\frac{\mathbf{n}\cdot\nabla s}{s(s-s_0)^{3/2}}, \quad (11)$$

where $\mathbf{n}$ is the normal vector to the boundary $\partial\Omega$.

D. The boundary value of saturation and steady states

The existence of a sharp boundary during the wetting of a dry porous material has been established experimentally in the case of particulate porous media [1, 4], in the experiments with the paper porous materials, a sharp boundary was also observed, though there are some differences discussed below.

As we have shown previously, the boundary value of saturation s_f is defined by the capillary pressure developed at the moving front, which in turn is conditioned in particulate porous media by the formation of bottleneck regions at the point of particle contacts [4]. In the fibrous porous media, such clear separation of the length scales generating the capillary pressure is not expected in a general case. Indeed, while the contact area between two particles vanishes when the bridge size shrinks and bottleneck regime of the contacts is achieved, the contact area between the fibres is expected to be still of the order of the fibre diameter R. In particulate porous media, this leads to a sharp cut off when propagation of the moving front practically stops. In the fibrous materials, this transition should be smoother, when the transport will be mostly conditioned by the smaller details of the fibres, for example intrafibre pores or other smaller elements of a fibre. For the first time, the absence of a clear cut off in the propagation dynamics was observed in the experiments on spreading of low vapour pressure liquids [30].

Further in the model development, we consider only the regime when the liquid bridges still exist, so that the minimal level s_0 is defined by fully saturated intrafibre structure. The boundary value then is always supposed

to be larger then the minimal value $s_f > s_0$ and should be defined by the length scale of the fibre details, δ_R.

To get an estimate of the typical values of the boundary pressure and the saturation, we assume that the pressure is generated by the capillaries with characteristic size of the order of δ_R. Then, for example for water, taking characteristic value of the surface tension $\gamma = 72\,\mathrm{mN/m}$ at 25° C, one can obtain that at $\delta_R = 1\,\mu\mathrm{m}$ the capillary pressure $P = \dfrac{2\gamma}{\delta_R} \approx 1.4 \times 10^5\,\mathrm{Pa}$. As a result, from (3), taking typical parameter values $L_e = 50\,\mathrm{mm}^{-1}$, $R = 7\,\mu\mathrm{m}$ and $\phi = 0.7$, parameter $s_f = 0.022$, that is $s_f \approx 2.2\,s_0$ at similar values of parameters.

One needs to note though, that in general the capillary pressure at the moving front may be generated by the fibre irregularities of smaller length scale than the average typical values responsible for the liquid accumulation in the fibres, that is contributing into the value of parameter s_0. So that parameters s_f and s_0 strictly speaking can be regarded as independent.

E. Microscopic model

To increase the predictive power of the macroscopic model and understand its range of parameters, one needs to turn to a microscopic view. Indeed, as it follows from the macroscopic formulation (9), to accurately predict liquid spreading at low saturation levels, one needs to know the main parameter $K = \kappa_m \frac{S_e}{S}$ contributing into the diffusivity, which, in turn, is defined by the connectivity of the porous paper network, that is by the parameter S_e/S. Connectivity is essentially a microscopic quantity, which can be only obtained using a microscopic network model.

The need to consider that microscopic dynamics becomes more apparent if we take into account that real porous materials are never absolutely homogeneous. So this would be informative to establish the sensitivity of the connectivity factor S_e/S to the conducting properties of the fibres and their distribution.

On the side, while modeling the transport in porous media using network models has shown, in general, that the methodology is stable and reliable, and is able to converge to the macroscopic results [31], the SFD has anomalous properties, such as a divergent coefficient of diffusion, so that this would be interesting and informative to compare the macroscopic and microscopic formulations in this special case.

The microscopic network model, we use here, is based on some simplifying assumptions. First of all, the microscopic network is essentially two-dimensional and consists of two elements: randomly placed nodes corresponding to the liquid bridges at the paper fibre crossings or at the branch points and the links corresponding to the fibres connecting the bridges, see Fig. 1. The random distribution of nodes has been generated using Voronoi algorithm and Delaunay triangulations [31, 32], when the original domain of simulations is tessellated into either triangles (three neighbours per node) or quadrilaterals (four neighbours per node), Fig. 1. At this stage, we are not going to engage the detailed pore-scale modelling, such as, for example, utilized in [33–37]. Such a simplification is fully justified since the flow at low saturation levels is predominantly over the surface elements, and there is no flow on the pore-scale level. Therefore, if we disregard the internal fibre structure or simply average, the network model appears to be exact. One needs also to take into consideration the cost of the low level simulations, which, to fully benefit, require high-resolution imaging of the porous system to make any tuning of the model and any comparison reasonable.

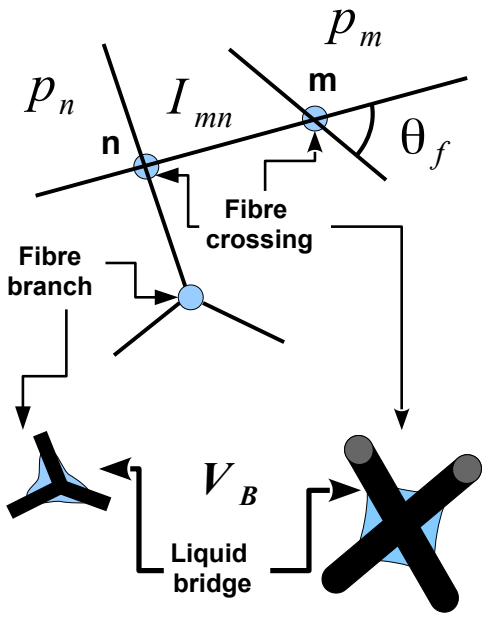

FIG. 1. Illustration of the microscopic network model configurations and parameters.

To obtain an equivalent to a three-dimensional case distribution of nodes in the two-dimensional network, the total number of nodes per unit area N_s in the two-dimensional case is set to be the same as the total number of crossings per unit area in a porous layer of thickness R, that is $N_s = N_c R$.

In what follows, we will use non-dimensional forms by normalizing distance, pressure, flux density and flux by R, p_0, $q_0 = \frac{\delta_R}{R}\frac{\kappa_m p_0}{\mu R}$ and $I_0 = \pi\delta_R \frac{\kappa_m p_0}{\mu}$ respectively. Then in non-dimensional form, designating non-dimensional variables by a bar, $\bar{N}_s = \bar{N}_c = \frac{8}{\pi}(1-\phi)^2$.

We further assume, according to (1), that at any node the liquid pressure is defined by the amount of the liquid

in the bridge, that is

$$\bar{p}_m = -\left(\frac{1}{\bar{V}_B^m}\right)^{1/2}, \tag{12}$$

where $\bar{V}_B^m$ is the normalized liquid volume at node m. At the same time, at non-equilibrium, the liquid flux between the nodes connected through the links is defined by the pressure difference. That is the liquid flux from node m to node n connected by the filament of length $\bar{L}_{mn}$ is proportional to the pressure difference between the nodes

$$\bar{I}_{mn} = -\alpha_{mn}\frac{\bar{p}_n - \bar{p}_m}{\bar{L}_{mn}}. \tag{13}$$

Such a relationship reflects the fact that the transport happens due to the surface flows in particular within the irregularities [28].

The coefficient of proportionality α_{mn} is a non-dimensional adjusting parameter, which takes into account the average shape of the fibres and their average ability to transport the liquid. The distribution of the fibre permeability is largely unknown, and this is not part of the current study. Therefore, to understand the impact of this distribution on macroscopic properties, parameter α_{mn} in our simulations was either a constant, $\alpha_{mn} = 1$, or was a random number uniformly distributed in the interval $0 \leq \alpha_{mn} \leq 1$, such that the average $< \alpha_{mn} >= 1/2$. Note, if all links would be of a cylindrical shape of diameter $\bar{D}_R = 1$ having a uniform liquid layer of thickness δ_R/R carrying the liquid flux, then all $\alpha_{mn} = 1$.

Liquid saturation can then be calculated as an average over some representative (that is containing many nodes) surface element with surface area $\bar{S}_0$. Since our prime concern here is permeability of the network, we will neglect the amount of the liquid stored in the links. That is,

$$s = \frac{\sum_k \bar{V}_B^k}{\phi \bar{S}_0},$$

where the summation is over all nodes within the surface element.

In a non-equilibrium state, the distribution of liquid in the network evolves in time with a time step Δt chosen to achieve numerical stability. After each time step, the total amount of the liquid at every node is calculated according to the mass balance, that is the mass change due to the total flux through the links connected to the node (13) and the amount at the previous time step.

Our prime concern here is a steady state when the flux density is constant. To obtain the macroscopic parameters, we setup a quasi one-dimensional problem, which is simulated using both the network model and an equivalent macroscopic model. This way, we are able to define macroscopic parameters, but also, as a side-product, to underpin the macroscopic model.

In the microscopic setup, the two-dimensional square area (side size $\bar{X} = 100$) is divided into equidistant strips in the x-direction (the direction of the diffusion) of a fixed width $\Delta_x = 2.5$. The nodes in the first and in the last strip are kept at a fixed liquid volume to emulate fixed boundary saturation levels. In the y-direction, zero flux boundary condition is set.

Equivalent macroscopic problem formulation

From the macroscopic point of view, the setup is supposed to be equivalent to a one dimensional problem for (9) with Dirichlet type boundary conditions, that is in a steady state

$$\frac{d}{d\bar{x}}\left\{\frac{ds}{d\bar{x}}s^{-3/2}\right\} = 0, \quad x \in (0, \bar{X}) \tag{14}$$

$$s(0) = s_1 \geq s_f, \quad s(\bar{X}) = s_2 \geq s_f.$$

The differential equation (14) has a general solution

$$s = \frac{1}{(\bar{C}_0 + \bar{C}_1\bar{x})^2}, \tag{15}$$

where

$$\bar{C}_0 = \frac{1}{\sqrt{s_1}}, \quad \bar{C}_1 = \frac{1}{\bar{X}}\left(\frac{1}{\sqrt{s_2}} - \frac{1}{\sqrt{s_1}}\right).$$

The constant flux density then

$$\bar{q}_s = -\frac{D_0\phi}{q_0 R}\frac{1}{s^{3/2}}\frac{ds}{d\bar{x}} = \bar{C}_1\frac{R}{\delta_R}\frac{S_e}{S}\sqrt{\frac{\bar{N}_c}{\phi}} \tag{16}$$

If the flux density is known in a steady state, the coefficient of diffusion can be obtained by fitting the observed profiles of $s(\bar{x})$ to get $\bar{C}_1$. So that the ratio of the area of entrances and exits S_e/S, the main connectivity parameter, is parametrized by the non-dimensional parameters δ_R/R and ϕ, since $\bar{N}_c = \bar{N}_c(\phi)$.

Steady state distributions and the network connectivity factor

In the simulations, the quasi one-dimensional network setup corresponding to the macroscopic model (15) evolved in time till the flux density arrived at a uniform distribution in the bulk within the tolerance of $5 - 10\%$. We used different total number of points in the fixed simulation domain (side size $\bar{X} = 100$) n_T and two types of networks, with three neighbours (triangular tessellation) and four neighbours (quadrilateral tessellation) per each node, namely, $n_T = 2300$, $\bar{N}_c = 0.23$ and $\phi = 0.7$, and $n_T = 6400$, $\bar{N}_c = 0.64$ and $\phi = 0.5$. The boundary values of saturation have been set to $s_1 = 0.1\%$ and to $s_2 = 20\%$ to cover the whole range, where the superfast

Number of nodes n_T	α_{mn}	ϕ	$\bar{N}_c$	$\bar{q}_s$	S_e/S
6400	1	0.5	0.64	-0.15 ± 0.008	$0.49\frac{\delta_R}{R}$
6400	Random	0.5	0.64	-0.056 ± 0.005	$0.17\frac{\delta_R}{R}$
2300	1	0.7	0.23	-0.038 ± 0.004	$0.25\frac{\delta_R}{R}$
2300	Random	0.7	0.23	-0.015 ± 0.001	$0.1\frac{\delta_R}{R}$

TABLE I. Simulation results in the steady state of the quasi-one-dimensional microscopic network model with triangular tessellation (three neighbours per a node) at different node densities, total number of nodes n_T. The saturation levels at the interval ends are fixed at $s_1 = 0.1\%$ and $s_2 = 20\%$. All data has been averaged over five independent simulations.

Number of nodes n_T	α_{mn}	ϕ	$\bar{N}_c$	$\bar{q}_s$	S_e/S
6400	1	0.5	0.64	-0.27 ± 0.01	$0.88\frac{\delta_R}{R}$
6400	Random	0.5	0.64	-0.11 ± 0.005	$0.36\frac{\delta_R}{R}$
2300	1	0.7	0.23	-0.075 ± 0.004	$0.49\frac{\delta_R}{R}$
2300	Random	0.7	0.23	-0.03 ± 0.002	$0.19\frac{\delta_R}{R}$

TABLE II. Simulation results in the steady state of the quasi-one-dimensional microscopic network model with quadrilateral tessellation (four neighbours per a node) at different node densities, total number of nodes n_T. The saturation levels at the interval ends are fixed at $s_1 = 0.1\%$ and $s_2 = 20\%$. All data has been averaged over five independent simulations.

regime may be expected. We have also used two different models for the link permeability parametrised by the non-dimensional coefficients α_{ij}, when either all $\alpha_{ij} = 1$ or they were randomly, but uniformly distributed in the interval $0 \leq \alpha_{ij} \leq 1$, such that the average $< \alpha_{ij} >= 1/2$.

What do we observe in simulations with the microscopic model? After reaching a steady state, when the flux density is constant in the flow domain, the distribution of pressure as a function of saturation, Fig. 2, was found to be in very good agreement with that anticipated in the macroscopic model (3), which is in a non-dimensional form

$$\bar{P} = -\sqrt{\frac{\bar{N}_c}{\phi}}\frac{1}{\sqrt{s}}. \tag{17}$$

As one can observe, Fig. 3, the saturation profiles $s(\bar{x})$ are in accord with those anticipated from the macroscopic model (15). One can conclude that on average the behaviour of the network model can be adequately described by the macroscopic equations.

The results of simulations involving network models with different parameters are summarized in Tables I and II. The connectivity factor S_e/S obtained in the simulations strongly depends (non-linearly) on the assumptions made about the conductivity of the links α_{mn} and, of course, on the node density $\bar{N}_c$, that is on the porosity ϕ. In general, the lower the porosity, the larger the conductivity, since more links are available to transfer the liquid.

The non-trivial behaviour is observed when at a fixed value of $\bar{N}_c$, the conductivity of the links becomes a random distribution. One can see from the tables, that while the mean value of $< \alpha_{mn} >= 0.5$, the connectivity factor S_e/S changes almost three times. Natural paper materials have rather random structures on the microscopic

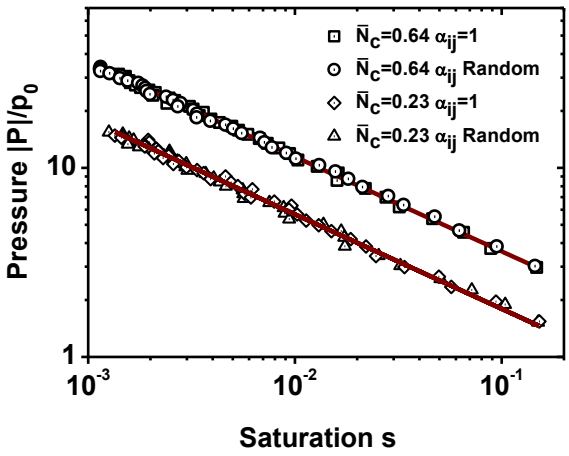

FIG. 2. Averaged, reduced capillary pressure $|P|/p_0$ as a function of saturation s in the model set-up with three nodal neighbours at $s_1 = 0.001$ and $s_2 = 0.2$, and at different values of $\bar{N}_c$, $\phi = 0.5$, $\bar{N}_c = 0.64$ and $\phi = 0.7$ and $\bar{N}_c = 0.23$, and different distributions of α_{ij}. The numerical data are shown by symbols and the solid lines (brown) indicate the fitting function $\frac{|P|}{p_0} = A_f s^{-1/2}$, $A_f = \sqrt{\frac{\bar{N}_c}{\phi}}$.

level, so that such changes should be taken into account. The result also implies that a small number of impurities obstructing the capillary flow may substantially reduce permeability of textured materials, as the SFD mechanism is particularly sensitive to the tortuosity of the pathways.

At the same time, the scaling factor of about 2, which is expected to occur in different microscopic connectivity models, that is when changing from the triangular tessellation (three neighbours per a node) to the quadrilateral

one (four neighbours per a node), is clearly observed in the average flux density values, Tables I and II.

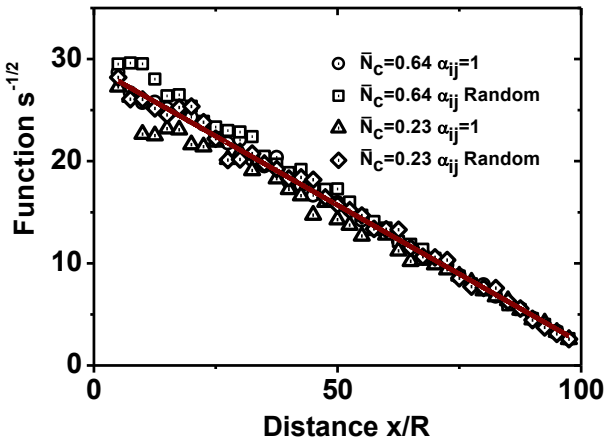

FIG. 3. Average saturation $s^{-1/2}$ as a function of the reduced distance $\bar{x} = x/R$ in the model set-up with three nodal neighbours at $s_1 = 0.001$ and $s_2 = 0.2$, and at different values of $\bar{N}_c$, $\phi = 0.5$, $\bar{N}_c = 0.64$ and $\phi = 0.7$ and $\bar{N}_c = 0.23$, and different distributions of α_{ij}. The numerical data are shown by symbols and the solid lines (brown) indicate the fitting function $s^{-1/2} = A_s + B_s\bar{x}$ at $A_s = 29.2 \pm 0.2$ and $B_s = -0.27 \pm 0.004$.

III. OBSERVATION OF LIQUID SPREADING IN PAPER POROUS MATERIALS

A. Experimental procedures

The experiments were designed to study interaction of a single liquid drop with a porous matrix, its subsequent penetration and spreading in the porous material within the framework of the witness card technique, which is widely used for accurate determination of the particle size distributions to assess the effectiveness of spraying in applications [38]. The emphasis in the current research was on the analysis of the general trends of liquid spreading at low saturation levels.

Our previous study of liquid dispersion in particulate porous media has shown that evolution of the wetting front in the later stages of the symmetric spreading, when the saturation level is below a critical value $s_c \approx 10\%$, follows a universal power law, when the wetting spot diameter $X(t)$ as a function of time t obeys $X(t) \propto t^{\beta}$, where the time is measured from the onset of the low saturation regime and the exponent $\beta = 1/(N_d + 1)$ is a function of the dimension N_d of the spreading domain only, that is independent of other parameters [4]. In particular, in our case, the spreading geometry in papers is symmetric and two-dimensional, $N_d = 2$, so that it is anticipated that $\beta = 1/3$.

To understand the origin of the universal exponent β, we consider a compactly supported symmetric spreading domain, which can be characterized by a single length scale parameter $X(t)$, for example the radius of a circle (in a two-dimensional geometry with $N_d = 2$) or of a sphere in a three-dimensional case at $N_d = 3$. Then, the total flux $\Pi(t)$ at the moving front $X(t)$ should be proportional to the moving front velocity and the radius X in a certain power related with the geometry of the domain, that is

$$\Pi(t) \propto X^{N_d - 1}\frac{dX}{dt}. \tag{18}$$

The second, non-trivial scaling

$$\Pi(t) \propto \frac{1}{X(t)}. \tag{19}$$

comes from the asymptotic analysis of the SFD model described by (9)-(11). The result is directly related with the Mexican hat distribution of saturation, Fig. 4, which is the typical solution of the SFD equation in a domain with a moving boundary, see details in [4].

Combining (18) and (19), one gets that

$$X^{N_d}\frac{dX}{dt} = const$$

and

$$X(t) \propto t^{1/(N_d+1)}. \tag{20}$$

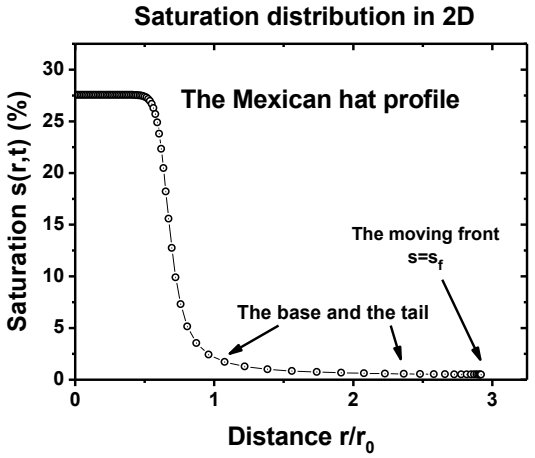

FIG. 4. Typical saturation distribution with a moving front $s = s(r,t)$ as a function of the reduced radius r/r_0 (r_0 is some initial length scale) obtained numerically at some $t > 0$ from the SFD model (9)-(11) in a symmetric two-dimensional geometry at $s_f = 0.5\%$ and $s_0 = 0.46\%$.

We note here that the power law dependence (20) has been clearly observed in both experiments in particulate porous media (in 1D and 3D symmetric setups) and numerical simulations of the SFD model with a moving boundary (in 1D, 2D and 3D symmetric formulations) [4]. It was found, the exponent is a very good indicator, which

is independent of the SFD model parameters, such as s_f and s_0. One can easily distinguish between the power law expected in fully saturated porous matrices and that in the case of the superfast diffusion at low saturation values. For example, $\beta = 1/2$ is predicted and observed in two-dimensional fully saturated cases [39].

Therefore, the power law dependence with the exponent $\beta = 1/(N_d + 1)$ is very characteristic for the low saturation regime of spreading [4]. Consequently, observation of the wetting spot evolution can reveal, in principle, the character of the diffusion process, and indicate that the diffusion process at low saturation levels in fibrous materials is also driven by the SFD mechanisms, as that in the particulate porous media.

On the other hand, as previous studies of liquid spreading in particulate porous media had clearly demonstrated, any detailed quantitative characterisation of the dispersion process at low saturation levels requires very detailed information about the porous media structure [2–4]. Therefore, detailed characterisation of the paper material, such as the micro-structure, and its relation with the transport properties will be the subject of future research, which may require a completely different approach.

In the experiments, a single liquid drop of a controlled volume (2.2 μL) has been dispatched from the drop generator whose position was adjustable. After separation from the generator head, the drop was accelerated by gravity up to its terminal velocity in the air. The variable positioning of the drop generator allowed for easy control of the drop impact velocity. The process of the falling drop splashing and spreading over the substrate was recorded by a high-speed video camera with the frame rate up to 20000 fps and a spatial resolution 50 pixel/mm. The recording was synchronized with a system of drop detection, which also made it possible to accurately measure the velocity at the time of the impact, Fig. 5. In the current study, we used two characteristic values of the impact velocity $u = 0.2\,\mathrm{m/s}$ and $u = 3.1\,\mathrm{m/s}$. To avoid any interference from a contact with a solid substrate, the paper sample was hanging on supporting rails in air.

The test liquid (2.2 μL drop) was neat tributyl phosphate (TBP, molar weight 266.32 g/mol), a low-volatility organophosphate compound dyed with Calco red or blue oil at different concentrations ($0.11\% - 0.5\%$ mass concentration respectively) to test fidelity of visualization.

This was important that the experimental liquid had extremely low equilibrium vapour pressure ($P_{ev} = 1.5 \times 10^{-1}\,\mathrm{Pa}$ at $20^\circ C$ [40]) to eliminate evaporation effects during the spreading. To introduce non-Newtonian effects and variations of viscosity, the neat (dyed) TBP solution was mixed with 3.8% (mass concentration) of Poly(Styrene-Butyl Methacrylate) (PSBMA).

The neat TBP solution has liquid viscosity $\mu = 3.88\,\mathrm{mPa \cdot s}$ and surface tension $\gamma = 28 \pm 1\,\mathrm{mN/m}$ measured in our laboratory at 20° C. The addition of the polymer into the pure TBP liquid resulted in substantial increase in the liquid viscosity $\mu_P \approx 340\,\mathrm{mPa \cdot s}$ at practically identical values of the surface tension $\gamma \approx 27\,\mathrm{mN/m}$, basically introducing non-Newtonian behaviour during the first, short lasting stage of the impact to avoid formation of satellite droplets, the so-called corona of the splashing droplet, Fig. 5. The details of the properties of the polymer solution, also used in viscoelastic aerobreakup studies, can be found in [41].

In all experiments, the visualization of the wet colored spot was performed in a regular white light, but with the contrast being sufficiently enhanced to resolve the low saturated tail of the distribution, Fig. 4. Indeed, in a separate set of long-term (about 6 hours) sensitivity experiments with pure TBP liquid dyed with blue oil on Whatman Grade 1 filter paper (nominal basis weight $87\,\mathrm{g/m^2}$, porosity $\approx 80\%$ and thickness $\approx 180\,\mu\mathrm{m}$), we were able to follow the spot to a state of rest, when the saturation value $s \approx 3\%$ was achieved on average (based on the assumption of the uniform distribution of the liquid within the spot), which is in accord with our theoretical estimate $s_f \approx 2.2\%$. To enhance the contrast of the images, they were post-processed by normalising the pixel intensity by that of the background (used for earlier times $t \leq 1000\,\mathrm{s}$) or, for longer times, by normalising the pixel intensity by that of the earlier images to see how the liquid is propagating with time, Fig. 6.

Qualitatively, as one can observe, there is a propagating tail, resembling the theoretical predictions of the SFD model, as in Fig. 4. But, this observation should be taken with caution, since the spot brightness may not be directly proportional to the saturation at low levels. The quantitative characterisation of the substrate saturation may require a completely different approach to obtain reliable measurements.

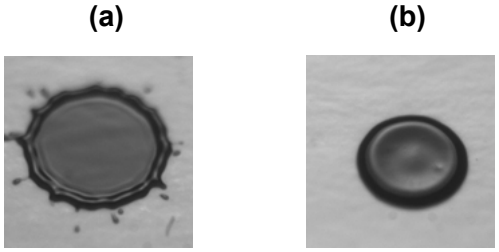

FIG. 5. Drop (volume 2.2 μL) impact at $t = 1.6\,\mathrm{ms}$ after the initial contact at the impact velocity 3.1 m/s: (a) neat TBP (b) TBP with 3.8% of PSBMA.

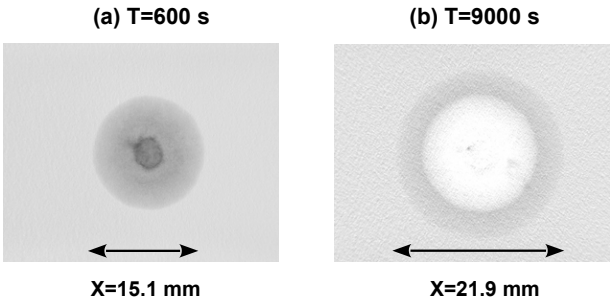

FIG. 6. Illustration of the wetting spots of the dyed (blue oil) neat TBP (2.2 μL drop) on Whatman Grade 1 filter paper in visible light at (a) $t = 600\,\mathrm{s}$ and (b) at $t = 9000\,\mathrm{s}$. To enhance the contrast of the wetting spots, the first image (a) had been post-processed by normalising the pixel intensity by the background value and the second image (b) had been post-processed by normalising the intensity by that of the image taken at an earlier moment at $t = 900\,\mathrm{s}$.

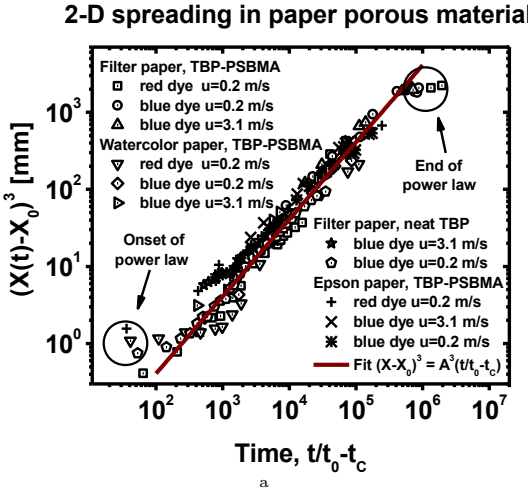

[a] The original data can be found in electronic supplementary material.

FIG. 7. The spot diameter X as a function of the reduced time t/t_0. Experimental data are shown by symbols at different impact velocities ($u = 0.2\,\mathrm{m/s}$ and $u = 3.1\,\mathrm{m/s}$), for different liquids (neat TBP and TBP with 3.8% PSBMA), different dyes (the Calco blue and red oils at 0.5% and 0.11% mass concentrations respectively) and different paper matrices (Epson, Filter and Watercolor papers). The solid line (brown) is the power-law fit $(X - X_0)^3 = A^3(t/t_0 - t_C)$ at $A = 0.16\,\mathrm{mm}$, $t_C = 10^3$ and $X_0 = 5.2\,\mathrm{mm}$. The data collapsed into a master curve by using the characteristic time scale: for the Filter paper and TBP+PSBMA $t_0 = 1/9 \pm 0.01\,\mathrm{s}$, the Watercolor paper and TBP+PSBMA $t_0 = 2 \pm 0.1\,\mathrm{s}$, for the Epson paper and TBP+PSBMA $t_0 = 1\,\mathrm{s}$ and for the Filter paper and neat TBP $t_0 = 1/900\,\mathrm{s}$.

B. Results and discussions

As we have already discussed, the detailed description of the liquid dispersion processes in paper porous materials, which requires microscopic information on the porous matrix, will be the subject of future research, so that here, we only analyse the general trends by observing the wetting spot diameter $X(t)$ as a function of time. Our prime concern is the long-time evolution of the spot diameter, which is shown in Fig. 7, when the spreading process is two-dimensional, that is when the spot diameter ($X \geq X_0 \sim 5\mathrm{mm}$) is much larger then the typical paper thickness ($50 - 180\,\mu\mathrm{m}$).

In the experiments, all drops were of a fixed volume of $2.2\,\mu$L. There were three different fibrous substrates: Epson paper ($80\,\mathrm{g/m^2}$), Watercolour paper ($300\,\mathrm{g/m^2}$) and Filter paper ($70\,\mathrm{g/m^2}$). It appears, though not surprisingly, that the long-time evolution of the wetting spot diameter (after some initial relaxation time t_C, that is at $t/t_0 > t_C$) on all samples in different conditions can be effectively reduced to a single master curve by renormalizing time t/t_0, where the characteristic time t_0 only depends on the liquid viscosity and the substrate material, Fig. 7, but, essentially, is independent of the initial conditions, such as the impact velocity, and the visualization materials (red or blue oils).

As one can clearly see from the figure, the spreading law $X(t/t_0) \propto (t/t_0 - t_C)^{1/3}$ is well observed at $t/t_0 \geq t_C$ indicating that indeed the spreading process after some initiation time t_C follows the superfast non-linear diffusion model. As one can also observe, the long-time evolution characteristic behaviour (the exponent β) is insensitive to the impact drop velocity, the type and concentration of the visualization liquid (red or blue Calco dyes), the substrate and liquid properties despite obvious difference in the initial conditions, Fig 5. That is, it is indeed universal, which is fully in line with the numerical simulations of the moving front in the SFD model, where parameter β in symmetric cases was seen to be only defined by the domain geometry.

One may also note that in spite of the non-Newtonian character of the polymer solution, the observed effect while switching from the neat TBP to its 3.8% polymer solution is simply down to the change in the zero shear rate viscosity from $\mu = 3.88\,\mathrm{mPa \cdot s}$ to $\mu_P \approx 340\,\mathrm{mPa \cdot s}$, corresponding to the change in t_0 from $t_0 = 1/900\,\mathrm{s}$ to $t_0 = 1/9\,\mathrm{s}$, assuming $t_0 \propto \mu$ according to (9).

A comparison with persistent liquids spreading

If one compares our observations with previous studies of persistent liquids spreading in paper materials, our data are in contrast to those observations. In two-dimensional cases, a different scaling law $X \propto t^{1/6}$ was observed instead of $X \propto t^{1/3}$ anticipated in the SFD model [30, 42]. Experiments in one-dimensional geometry [30] revealed $X \propto t^{1/3}$, while the SFD model predicts

the scaling $X \propto t^{1/2}$.

Despite different exponents, there is no contradiction, in our view. The main fundamental difference, we speculate, may come from the definition of the wetting spot area, and therefore the position of the moving front. To illustrate this point, consider the typical (in any geometry) distribution of the SFD model, which is shown in Fig. 4 in a two-dimensional case. In the previous studies, the boundary position was likely to be ascribed to the base of the distribution (based on the visualization method), where the saturation drops down to a very low, but still a finite value, while we followed, to some extent, the tip of the tail. So that experimentally, within certain accuracy, it could be possible to define the moving front position in that way, but this would lead to misinterpretation of the driving mechanism of the spreading. It is informative to note, that in numerical simulations of the SFD model, the dynamics of the base of the distribution was indeed found to be much slower and indeed to follow a scaling law close to $X \propto t^{1/6}$ in a two-dimensional case and $X \propto t^{1/3}$ in a one-dimensional geometry.

We believe that it was essential that we were able to observe the wider wet region including the distribution tail, Fig. 4, otherwise the measurements would result in underestimation of the wet area [4]. This is another example of the peculiar fundamental properties of the superfast diffusion, which must be taken into account when dealing with this phenomenon.

CONCLUSIONS

In conclusion, the diffusion process at low saturation levels in fibrous porous materials is shown to be fully compatible with that anticipated from the macroscopic SFD model. The long-time behaviour is well consistent with the model predictions, but further work is required to link microscopic parameters of the fibrous porous matrix with the macroscopic parameters of the evolution to enhance the predictive power of the model.

What is important for applications is that the long-time behaviour is insensitive to the initial conditions (impact velocity and the character of the initial splash), but only depends on the liquid properties (viscosity) and the properties of the substrate through a single parameter t_0.

It is also important, that the character of the evolution law is universal, such that the exponent $\beta = 1/3$, and it can only be influenced by the geometry of the diffusion domain, its dimension N_d, $\beta = 1/(N_d + 1)$.

Authors' contributions

All authors were involved in the preparation of the manuscript. AL and TT conceived of the study, designed the study, coordinated the study and helped draft the manuscript. PS and TP carried out numerical analysis and analytical studies of the model, participated in data analysis and critically revised the manuscript. VM carried out the experimental work, participated in the design of the study and in data analysis, and critically revised the manuscript. All authors have read and approved the final manuscript. All authors gave final approval for publication and agree to be held accountable for the work performed therein.

Competing interests.

The authors declare that they have no competing interests.

Funding.

The research was partially supported through the Royal Thai Government scholarship and the EPSRC Grant EP/P000835/1.

Acknowledgments.

The authors thank the referees for their valuable comments. We are grateful for their constructive remarks, which led to a significant improvement to the manuscript.

[1] A.V. Lukyanov, M.M Sushchikh, M.J. Baines and T.G Theofanous, Superfast Nonlinear Diffusion: Capillary Transport in Particulate Porous Media *Phys. Rev. Lett.* **109**, 214501, (2012)

[2] Sirimark, P.; Lukyanov, A.V. and Pryer, T., Surface permeability of porous media particles and capillary transport *Eur. Phys. J. E* **41**, 106, (2018)

[3] Sirimark, P.; Lukyanov, A.V. and Pryer, T., Surface permeability of particulate porous media *Transport in Porous Media* **130**, 637–654, (2019)

[4] Lukyanov, A.V.; Mitkin, V.V.; Theofanous, T.G. and Baines, M.J., Capillary transport in particulate porous media at low levels of saturation *J. Appl. Phys.* **125**, 185301, (2019)

[5] Vazquez, J.L., *Smoothing and Decay Estimates for Nonlinear Diffusion Equations—Equations of Porous Medium Type* (Oxford University Press, New York, 2006)

[6] Vazquez, J.L., *The Porous Medium Equation: Mathematical Theory* (Oxford University Press, 2006)

[7] Mualem, Y., A New Model for Predicting the Hydraulic Conductivity of Unsaturated Porous Media *Water Resources Research* **12**, 513–522, (1976)

[8] M. Th. van Genuchten, A Closed-form Equation for Predicting the Hydraulic Conductivity of Unsaturated Soils

Soil Sci. Soc. Am. J. **44**, 892, (1980)
[9] M. Scheel, R. Seemann, M. Brinkmann, M. D.I. Michiel, A. Sheppard, B. Breidenbach and S. Herminghaus, Morphological clues to wet granular pile stability *Nature Mater.* **7**, 189, (2008)
[10] M. Scheel, R. Seemann, M. Brinkmann, M. D.I. Michiel, A. Sheppard and S. Herminghaus, Liquid distribution and cohesion in wet granular assemblies beyond the capillary bridge regime *J. Phys. Condens. Matter* **20**, 494236, (2008)
[11] Novy, R.A.; Toledo, P.G.; Davis, H.T. and Scriven, L.E., Capillary Dispersion in Porous Media at Low Wetting Phase Saturations *Chem. Eng. Sci.* **44**, 1785–1797, (1989)
[12] Rosenau, P., Fast and Superfast Diffusion Processes *Phys. Rev. Lett.* **74**, 1056–1059, (1995)
[13] Xu, W.; Liang, Y.; Chen, W. and Cushman, J.H., A spatial structural derivative model for the characterization of superfast diffusion/dispersion in porous media *Int. J. Heat Mass Transf.* **139**, 39–45, (2019)
[14] G.A. Posthuma-Trumpie; J. Korf and A. van Amerongen, Lateral flow (immuno)assay: its strengths, weaknesses, opportunities and threats. A literature survey *Anal. Bioanal. Chem.* **393**, 569–582, (2009)
[15] K. Yamada, H. Shibata, K. Suzuki and D. Citterio, Toward practical application of paper-based microfluidics for medical diagnostics: state-of-the-art and challenges *Lab Chip* **17**, 1206–1249, (2017)
[16] L.-L. Shen, G.-R. Zhang and B.J.M. Etzold, Paper-Based Microfluidics for Electrochemical Applications *ChemElectroChem* **7**, 10–30, (2020)
[17] K.J. Niskanen and M.J. Alava, Planar Random Networks with Flexible Fibers *Phys. Rev. Lett.* **73**, 3475, (1994)
[18] W.W. Sampson, The Statistical Geometry of Fractional Surface Area in Random Fibre Networks *J. Pulp Paper Sci.* **29**, 412, (2003)
[19] S.J. Eichhorn and W.W. Sampson, Statistical geometry of pores and statistics of porous nanofibrous assemblies *J. R. Soc. Interface* **2**, 309–318, (2005)
[20] M. Alava and K. Niskanen, The physics of paper *Rep. Prog. Phys.* **69**, 669-723, (2006)
[21] M. Rasi, Permeability properties of paper materials *Research report. Department of Physics, University of Jyväskylä no. 13/2013* (2013)
[22] S. Herminghaus, Dynamics of wet granular matter *Adv. Phys.* **54**, 221, (2005)
[23] A. Sauret, A.D. Bick, C. Duprat and H.A. Stone, Wetting of crossed fibers: Multiple steady states and symmetry breaking *EPL* **105**, 56006, (2014)
[24] A. Sauret, F. Boulogne, B. Soh, E. Dressaire and H.A. Stone, Wetting morphologies on randomly oriented fibers *Eur. Phys. J. E* **38**, 62, (2015)
[25] M. Soleimani, R.J. Hill and T.G.M. van de Ven, Capillary Force between Flexible Filaments *Langmuir* **31**, 8328–8334, (2015)
[26] F.M. Orr, L.E. Scriven and A.P. Rivas, Pendular rings between solids: meniscus properties and capillary force *J. Fluid Mech.* **67**, 723-742, (1975)
[27] Halsey, T.C. and Levine, A.J., How Sandcastles Fall *Phys. Rev. Lett.* **80**, 3141-3144, (1998)
[28] R.R. Rye, F.G. Yost and E.J. O'Toole, Capillary flow in irregular surface grooves *Langmuir* **14**, 3937, (1998)
[29] S. Whitaker, Advances in Theory of Fluid Motion in Porous Media *Ind. Eng. Chem.* **61**, 14–28, (1969)
[30] T. Gillespie, The Spreading of Low Vapor Pressure Liquids in Paper *J. Colloid. Sc.* **13**, 32–50, (1958)
[31] Blunt, M.J. and King, P., Relative Permeabilities from Two- and Three-Dimensional Pore-Scale Network Modelling *Trans. Porous Media* **6**, 407–433, (1991)
[32] Fortune, S., Voronoi diagrams and Delaunay triangulations *Computing in Euclidean geometry* (World Scientific, Amsterdam, 1995)
[33] J.J. Meyers and A.I. Liapis, Network Modeling of the Convective Flow and Diffusion of Molecules Adsorbing in Monoliths and in Porous Particles Packed in a Chromatographic Column *J. Chromatogr. A* **852**, 3–23, (1999)
[34] Blunt, M.J., Flow in porous media — pore-network models and multiphase flow *Current Opinion in Colloid & Interface Science* **6**, 197–207, (2001)
[35] Valvatne, P.H. and Blunt, M.J., Predictive pore-scale modeling of two-phase flow in mixed wet media *Water Resour. Res.* **40**, W07406, (2004)
[36] A. Nabovati, E.W.; Llewellin and A.C.M. Sousa, A general model for the permeability of fibrous porous media based on fluid flow simulations using the lattice Boltzmann method *Composites: Part A* **40**, 860–869, (2009)
[37] Blunt, M.J.; Lin, Q.; Akai, T.; Bijeljic, B., A thermodynamically consistent characterization of wettability in porous media using high-resolution imaging *J. Colloid. Interface Sci.* **552**, 59–65, (2019)
[38] A. Sundaram, K.M.S. Sundaram and J.M. Leung, Droplet spreading and penetration of non-aqueous pesticide formulations and spray diluents in Kromekote cards *Transactions of the ASAE* **34**, 1941–1951, (1991)
[39] J. Xiao, H.A. Stone and D. Attinger, Source-like Solution for Radial Imbibition into a Homogeneous Semi-infinite Porous Medium *Langmuir* **28**, 4208–4212, (2012)
[40] Skene, W.G. and Krzymien, M.E., Vapor pressure of TBP *J. Chem. Eng. Data* **40**, 394–397, (1995)
[41] T.G. Theofanous, V.V. Mitkin, and C.L. Ng, The physics of aerobreakup. III. Viscoelastic liquids *Phys. Fluids* **25**, 032101, (2013)
[42] D. Danino and A. Marmur, Radial Capillary Penetration into Paper: Limited and Unlimited Liquid Reservoirs *J. Colloid. Interface Sc.* **166**, 245–250, (1994)